JVST A
Journal of Vacuum Science & Technology A

Thermal stability of band offsets of NiO/GaN

Cite as: J. Vac. Sci. Technol. A **40**, 053401 (2022); https://doi.org/10.1116/6.0002033
Submitted: 21 June 2022 • Accepted: 29 June 2022 • Published Online: 29 July 2022

Xinyi Xia, Jian-Sian Li, Chao-Ching Chiang, et al.

View Online Export Citation CrossMark

ARTICLES YOU MAY BE INTERESTED IN

Demonstration of 4.7 kV breakdown voltage in NiO/β-Ga_2O_3 vertical rectifiers
Applied Physics Letters **121**, 042105 (2022); https://doi.org/10.1063/5.0097564

Erratum: "Practical guide for curve fitting in x-ray photoelectron spectroscopy" [J. Vac. Sci. Technol. A 38, 061203 (2020)]
Journal of Vacuum Science & Technology A **40**, 057001 (2022); https://doi.org/10.1116/6.0002004

Characterizations of two-dimensional materials with cryogenic ultrahigh vacuum near-field optical microscopy in the visible range
Journal of Vacuum Science & Technology A **40**, 040801 (2022); https://doi.org/10.1116/6.0001853

© 2022 Author(s).

JVST A
Journal of Vacuum Science & Technology A
ARTICLE
avs.scitation.org/journal/jva

Thermal stability of band offsets of NiO/GaN

Cite as: J. Vac. Sci. Technol. A **40**, 053401 (2022); doi: 10.1116/6.0002033
Submitted: 21 June 2022 · Accepted: 29 June 2022 ·
Published Online: 29 July 2022

View Online Export Citation CrossMark

Xinyi Xia,[1] Jian-Sian Li,[1] Chao-Ching Chiang,[1] Timothy Jinsoo Yoo,[2] Fan Ren,[1] Honggyu Kim,[2] and S. J. Pearton[2,a)]

AFFILIATIONS

[1]Department of Chemical Engineering, University of Florida, Gainesville, Florida 32606
[2]Department of Materials Science and Engineering, University of Florida, Gainesville, Florida 32606

[a)]**Electronic mail:** spear@mse.ufl.edu

ABSTRACT

NiO is a promising alternative to p-GaN as a hole injection layer for normally-off lateral transistors or low on-resistance vertical heterojunction rectifiers. The valence band offsets of sputtered NiO on c-plane, vertical geometry homoepitaxial GaN structures were measured by x-ray photoelectron spectroscopy as a function of annealing temperatures to 600 °C. This allowed determination of the band alignment from the measured bandgap of NiO. This alignment was type II, staggered gap for both as-deposited and annealed samples. For as-deposited heterojunction, $\Delta E_V = 2.89$ eV and $\Delta E_C = -2.39$ eV, while for all the annealed samples, ΔE_V values were in the range of 3.2–3.4 eV and ΔE_C values were in the range of −(2.87–3.05) eV. The bandgap of NiO was reduced from 3.90 eV as-deposited to 3.72 eV after 600 °C annealing, which accounts for much of the absolute change in $\Delta E_V - \Delta E_C$. At least some of the spread in reported band offsets for the NiO/GaN system may arise from differences in their thermal history.

Published under an exclusive license by the AVS. https://doi.org/10.1116/6.0002033

I. INTRODUCTION

There is considerable recent interest in developing GaN-based high efficiency power converters with much lower switching losses than Si devices.[1–12] GaN homostructures or AlGaN/GaN heterostructures also allow devices with smaller surface area and higher operating frequencies than Si. In addition, there can also be a reduction in the size of the associated parasitic inductors and capacitors, which lead to miniaturized, ultra-high-density power converters[1–12] and terahertz frequency multipliers.[13] GaN power devices are already commercialized for applications such as fast chargers, electric vehicles, data centers, and aerospace. The Huang Material figure-of-merit, $E_C\mu^{0.5}$, is a reliable predictor of power density in a variety of power converter types, where E_C is the critical electric field for breakdown and μ is the electron mobility.[1–3] Since E_C scales approximately as $E_G^{2.7}$, where E_G is the bandgap, more than an order of magnitude improvement in power density is enabled by the use of GaN compared to Si.[14–17] GaN also has numerous advantages for power amplifiers and high-power switch technology for 5G-Advanced and 6G communications and base station radios, while reducing the system size and weight. A relatively new application is power electronics for electrified aircraft. The specific power of power electronic inverters for aircraft applications is approaching 20 kW/kg, and the peak efficiency can be above 99%.[18,19]

One drawback is the relatively low hole concentrations obtainable in p-GaN, needed to provide p-gates in normally-off (enhancement mode) lateral transistors, which are more advantageous for power applications,[14] or the p-side of vertical pin diodes. Recently, several reports have appeared on replacing p-GaN with p-type NiO.[20–22] This demonstrates higher hole concentration with similar work function to p-GaN and has been used to demonstrate normally off p-NiO-gated AlGaN/GaN High Electron Mobility Transistors (HEMTs).[22] Another potential advantage is added flexibility in designing junction termination extension and p-type guard rings as well as the fact that p-n junctions can readily afford avalanche breakdown, a key capability in many applications.[23–28] Normally-off devices require the application of a positive voltage to the gate to turn the device on.[1,2] Another common way to achieve a normally-off device is by tuning AlGaN/GaN polarization to modulate the 2DEG by changing the doping or thickness of the AlGaN layer.[1–7] Commercial GaN normally-off devices are based either on the cascode or on the p-GaN technology.[1–3] NiO has also been used as a hole injection layer on ZnO[29–32] and Ga_2O_3 heterojunction devices.[33–44]

A key aspect in the performance of NiO/GaN devices is the thermal stability of the band alignment of the heterojunction. Gou *et al.*[9] reported that there was interfacial reconstruction of the

Published under an exclusive license by the AVS

p-NiO/AlGaN interface and an increase in interface states due to formation of a thin c-Al_2O_3 insulating layer after 500 °C annealing. This change in the conduction-band profile at the interface produced a significant change in device operation characteristics. The valence band offset at the NiO/AlGaN interface was 1.64 eV prior to annealing and 1.86 eV after 500 °C annealing. The band alignment was staggered type-II in both the initial and annealed NiO/AlGaN interfaces. Similar studies have been reported by several groups for NiO on pure GaN, with a significant spread in respective band offsets.[45–47]

If NiO is to be useful as a hole injection layer on GaN, then the thermal stability of NiO/GaN heterointerfaces needs to be established so that the processing sequence can be optimized. In this paper, we report measurements of the band alignment as a function of post-deposition annealing temperature up to 600 °C and see a monotonic increase in the values of the staggered band offsets with annealing temperature.

II. EXPERIMENT

We used vertical rectifier structures for the measurement of band alignments. These were purchased from Kyma Technologies and consisted of a 8 μm thick, nominally undoped epitaxial layer grown by hydride vapor phase epitaxy (HVPE) with carrier concentration of 5×10^{15} cm^{-3} on a c-plane, Si-doped n$^+$-GaN substrate. NiO layers were deposited by radio-frequency (RF) magnetron sputtering at <100 °C temperature. The RF power was 150 W, and the purity of the dual NiO targets was 99.99%. During deposition, the chamber pressure was 3 m Torr in an Ar/O_2 mixed ambient and the deposition rate was 0.2 Å s^{-1}. The Ar/O_2 ratio was used to control the doping in the NiO at $\sim 10^{19}$ cm^{-3} with a mobility of <1 cm^2 V^{-1} s^{-1}. These values are consistent with literature values.[48] Three different types of sample were prepared, namely, a thick layer (60 nm) of NiO deposited on quartz, the bare GaN samples, and a heterostructure consisting of a thin 5–10 nm NiO layer on GaN. A cross-sectional high-angle annular dark field (HAADF) scanning transmission electron microscope (STEM) image of the latter is shown in Fig. 1. Given that HAADF-STEM images exhibit atomic weight sensitivity, the dark contrast at the interface of NiO and GaN is likely due to sputtering-induced disorder during deposition of NiO. The interface itself is atomically abrupt with no extended defects into the substrate or the film.

The TEM sample was fabricated along the [21$\bar{1}$0] zone axis with an FEI Helios Dualbeam Nanolab 600 focused ion beam (FIB) system. HAADF-STEM imaging was performed on the aberration-corrected Themis Z (Fisher Scientific) at 200 kV with a 30 pA screen current.

The bandgaps of NiO for as-deposited films and those after annealing at different temperatures were obtained using the UV-Vis (Perkin-Elmer Lambda 800 UV/Vis spectrometer) absorbance spectrum. Tauc plots were used to calculate the bandgap of NiO.°

The band alignments were obtained using x-ray photoelectron spectroscopy (XPS).[49] The XPS system was a Physical Instruments ULVAC PHI, with an Al x-ray source (energy 1486.6 eV, source power 300 W), analysis size of 100 μm diameter, a take-off angle of 50°, and an acceptance angle of ±7°. The electron pass energy was

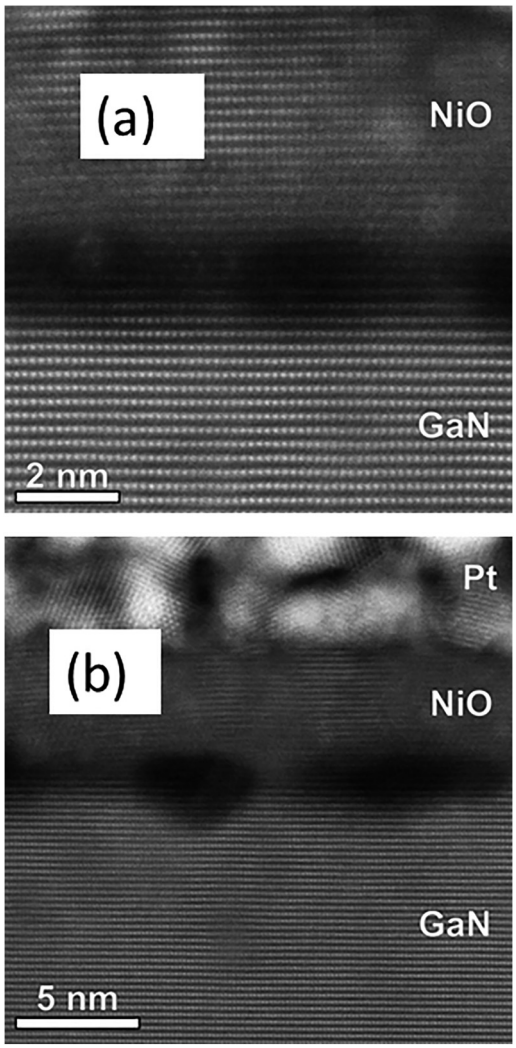

FIG. 1. Atomic-resolution HAADF-STEM images of the NiO/GaN heterojunction at two different magnifications. The GaN substrate remains fairly pristine (a) while the NiO film is polycrystalline and ~5 nm in thickness. The interface is atomically abrupt, and the dark contrast is likely due to sputtering-induced disorder (b).

23.5 eV for high-resolution scans and 93.5 eV for survey scans. The total energy resolution of this XPS system is about 0.5 eV, and the accuracy of the observed binding energy is within 0.03 eV. The core levels and valence band maxima (VBM) positions were measured from thick NiO layers and in the epitaxial GaN. These same core levels were remeasured in the NiO/GaN heterojunction. The acquired XPS spectra were calibrated using the C 1s peak at 284.8 eV and while this is not always reliable for calibration,[50] any charging effect/band bending effect causes the peaks to shift by the same amount of energy.[51] This absolute binding energy is, therefore, not important in measuring the band structure. We subtracted

Published under an exclusive license by the AVS

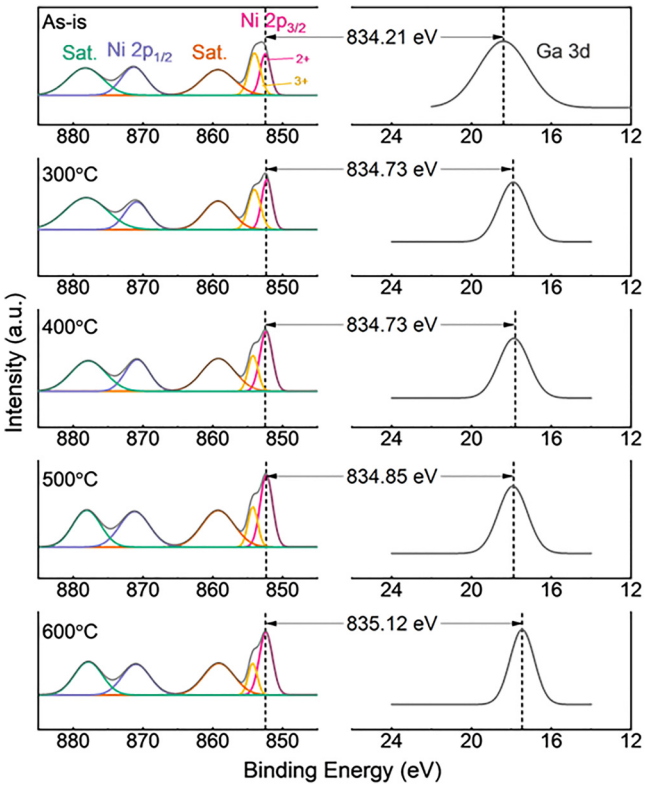

FIG. 2. ΔCore level calculations for interfaces of thin NiO/GaN as-deposited and annealed at different temperatures from 300–600 °C.

the BE of Ga 2*p* and Ni 2*p* to eliminate possible charging effects on the band bending, but in any case, sample charging was not an issue in these conducting samples and was not observed.

The shift of the core-level binding energy locations (ΔECL) within the heterostructure determines the valence band offset

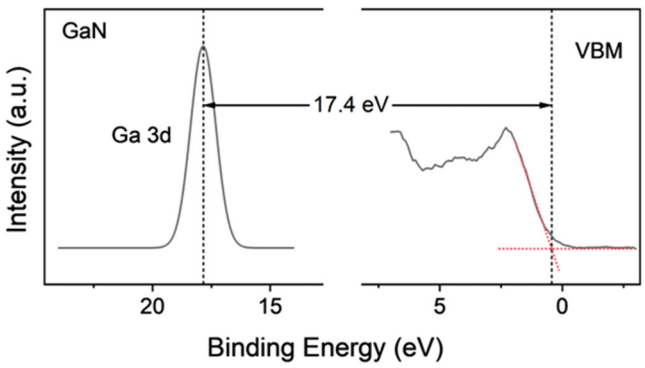

FIG. 3. High-resolution XPS spectra for the vacuum-core delta region of the reference GaN sample.

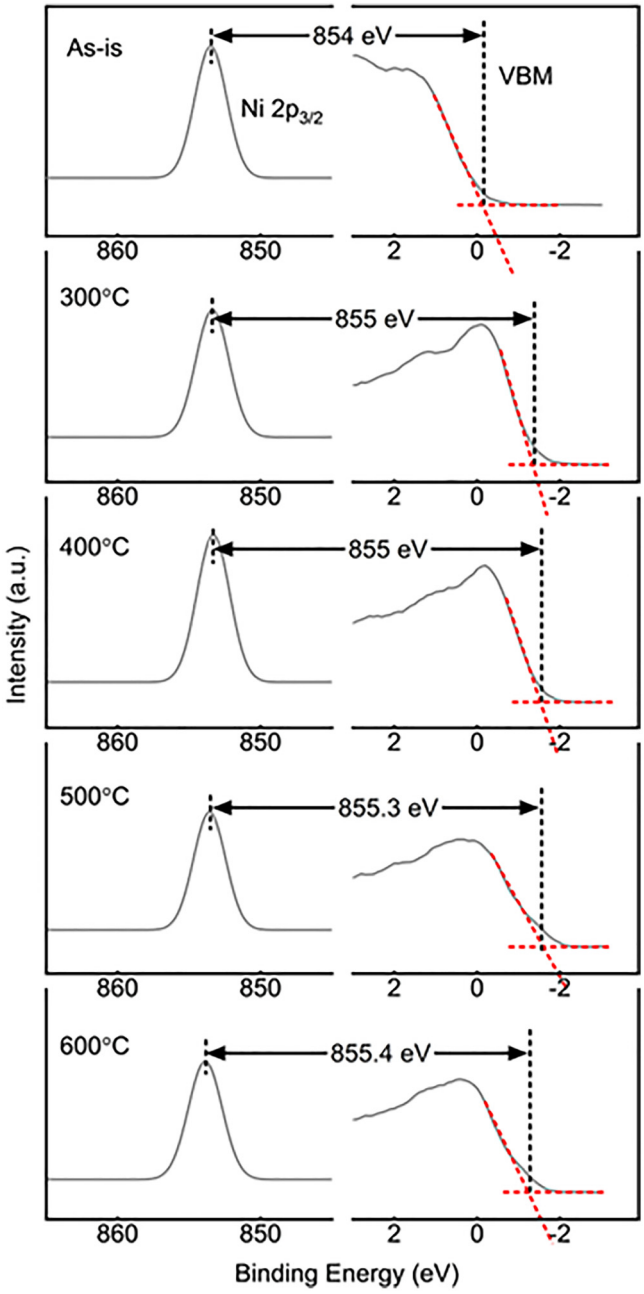

FIG. 4. Core-VBM calculations for thick NiO film as-deposited and annealed at different temperatures from 300 to 600 °C.

(ΔE_V) from[49,52,53]

$$\Delta E_V = \Delta ECL + (E_{Core} - E_{VBM})_{Ref.\ GaN} - (E_{Core} - E_{VBM})_{Ref.\ NiO}.$$

The associated conduction band offsets, ΔE_C, were obtained by subtracting valence band offsets from the bandgaps of NiO and GaN.

Published under an exclusive license by the AVS

TABLE I. Summary of measured core levels (eV) for NiO and a heterostructure of NiO deposited on GaN as a function of post-deposition annealing temperature.

	Bulk NiO			NiO/GaN heterojunction		
Anneal T (°C)	VBM	Core level peak (Ni 2p)	Core-VBM	Core level peak (Ga 3d)	Core level peak (Ni 2p)	△Core level
As-deposited	−0.6	853.4	854.0	18.27	852.48	834.21
300	−1.8	853.2	855.0	17.72	852.45	834.73
400	−1.9	853.1	855.0	17.71	852.44	834.73
500	−1.9	853.4	855.3	17.7	852.55	834.85
600	−1.7	853.7	855.4	17.37	852.49	835.12

III. RESULTS AND DISCUSSION

The bandgaps of NiO were measured before and after annealing for 5 min at 300–600 °C under an O_2 ambient. The bandgaps extracted from the Tauc plots were 3.90 eV (as-deposited), 3.84 eV (300 °C), 3.76 eV (400 °C), 3.74 eV (500 °C), and 3.72 eV (600 °C). The as-deposited value is consistent with the range of values reported in the literature.[48] The small changes with annealing are also consistent with the literature.[48]

The high-resolution XPS spectra for the vacuum-core delta regions of GaN are shown in Fig. 2 for as-deposited samples and those annealed at 300–600 °C. High-resolution XPS spectra for the vacuum-core delta region of the reference GaN sample are shown in Fig. 3.

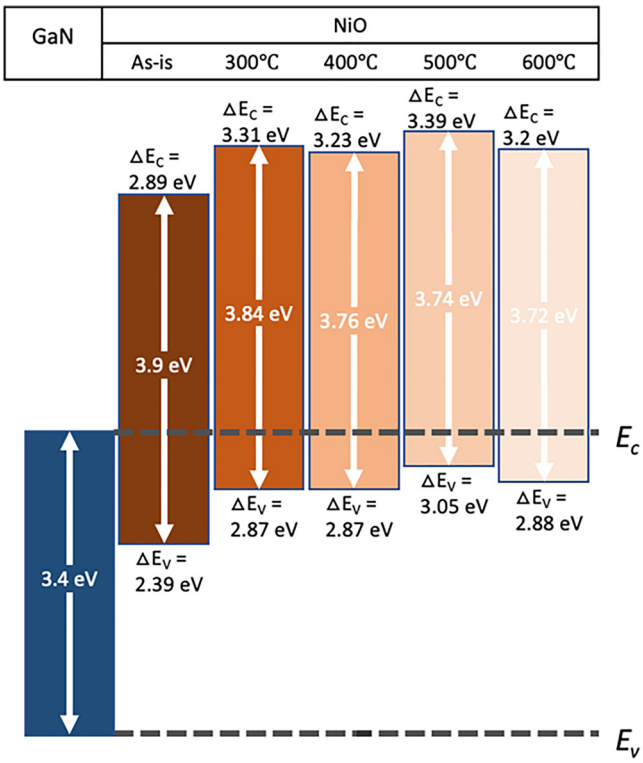

FIG. 5. Schematic of band alignments for NiO/GaN as a function of post-deposition annealing temperature from 300 to 600 °C.

The ΔE_V values are obtained from the shift of core levels for NiO/GaN heterojunction samples.[49,52,53] The XPS spectra from which we extracted the core energy differences to VBM for thick NiO layers after different annealing temperatures are shown in Fig. 4 and the peak position data are summarized in Table I. The corresponding valence band offsets were $\Delta E_V = 2.39$ eV (as-deposited), 2.87 eV (300 °C), 2.87 eV (400 °C), 3.05 eV (500 °C), and 2.88 eV (600 °C). The respective conduction band offsets are then −2.89 eV (as-deposited), −3.31 eV (300 °C), −3.23 eV (400 °C), −3.39 eV (500 °C), and −3.2 eV (600 °C). The error bars were ±0.025 eV for all these values.[52,53]

Figure 5 shows the annealing temperature dependence of the band alignment of NiO on GaN. The band alignment is staggered, type II in all cases. The band offsets increase monotonically with annealing temperature and will not provide any barrier to either electrons or holes moving into the GaN. Gong *et al.*[9] reported a similar trend for NiO on $Al_{0.25}Ga_{0.75}N$, with a type II alignment, a valence band offset of 1.64 eV, and a conduction band offset of 1.37 eV for the as-deposited case, and an increase in these values to $\Delta E_V = 1.86$ eV and $\Delta E_C = 1.63$ eV after annealing at 500 °C is observed. This was speculated to be due to O atom incorporation replacing N sites at the NiO/AlGaN interface and also the formation of a thin Al_2O_3 layer.[9] The latter is obviously absent in our samples, which do not include AlGaN. Zhang *et al.*[45] reported valence and conduction band offsets of 1.63 and 1.38 eV, respectively, for reactively sputtered NiO on AlGaN/GaN heterostructures. The deposition temperature was below 30 °C in this case.[45] Baraik *et al.*[46] determined ΔE_V and ΔE_C values of 1.4 and 1.9 eV for NiO/GaN where NiO was deposited by pulsed laser deposition at 600 °C, while Li *et al.*[47] presented the VBO and CBO values of

TABLE II. Reported values for band offsets of NiO on GaN or AlGaN.

NiO deposition	ΔEc (eV)	ΔE_V (eV)	Reference
PLD, 600 °C	−1.9	1.4	46
Reactive sputtering, RT	−1.38	1.63	45
E beam Ni, oxidation at 500 °C	−1.5	1.2	47
*$Al_{0.25}Ga_{0.75}N$, rf magnetron, RT	−1.63	1.86	9
Magnetron sputtering	−2.34	2.89	This work

Published under an exclusive license by the AVS

1.2 and 1.5 eV for NiO/GaN where the NiO was formed by oxidation of Ni at 500 °C. These results are summarized in Table II, which emphasizes the large spread in reported values. However, all of them agree on the type of alignment. Figure 5 appears to show an apparent saturation of the change in magnitude of band offsets, at least up to 600 °C. Given that Ohmic contact annealing temperatures for GaN are much higher than this temperature, the NiO would need to be deposited after Ohmic contact formation. It is also noteworthy from the literature that higher deposition temperatures produce band offset values closest to our values after annealing.

The large variation in deposition or formation temperatures for NiO in the previous work may explain the spread in reported values of valence and conduction band offsets. Hays *et al.*[53] summarized possible reasons for variations in band offsets between nominally similar systems, including different strain, interfacial disorder and contamination, stoichiometry, and chemical bonding variations. At this stage, the exact cause cannot be isolated and awaits more experiments where deposition conditions are carefully controlled.

IV. CONCLUSIONS

The spread in reported values for valence band offsets, which vary from 1.2 to 2.39, and conduction band offsets, which vary from −(1.3–2.89) eV, shows that there is still additional work necessary to understand the NiO/GaN interface and its variability with the deposition method, thermal budget, and the surface cleaning procedure. The reported variations in reported band offsets in this system requires examination of less energetic deposition methods than sputtering, since disruption to the interfacial region is known to affect band alignment.

ACKNOWLEDGMENTS

The work at UF was performed as part of Interaction of Ionizing Radiation with Matter University Research Alliance (IIRM-URA), sponsored by the Department of the Defense, Defense Threat Reduction Agency under Award No. HDTRA1-20-2-0002. The content of the information does not necessarily reflect the position or the policy of the federal government, and no official endorsement should be inferred. The work at UF was also supported by the National Science Foundation (NSF) under No. DMR 1856662 (James Edgar).

AUTHOR DECLARATIONS

Conflicts of Interest

The authors have no conflicts to disclose.

Author Contributions

Xinyi Xia: Conceptualization (equal); Data curation (equal); Investigation (equal); Writing – original draft (equal). **Jian-Sian Li:** Conceptualization (equal); Data curation (equal); Writing – original draft (equal). **Chao-Ching Chiang:** Data curation (equal); Formal analysis (equal); Writing – original draft (equal). **Timothy Jinsoo Yoo:** Conceptualization (equal); Data curation (equal); Methodology (equal); Writing – original draft (equal). **Fan Ren:** Conceptualization (equal); Writing – original draft (equal). **Honggyu Kim:** Conceptualization (equal); Data curation (equal); Writing – original draft (equal). **S. J. Pearton:** Conceptualization (equal); Data curation (equal); Writing – original draft (equal); Writing – review & editing (equal).

DATA AVAILABILITY

The data that support the findings of this study are available within the article.

REFERENCES

[1]H. Fu *et al.*, Mater. Today **49**, 296 (2022).
[2]M. Meneghini *et al.*, J. Appl. Phys. **130**, 181101 (2021).
[3]H. Fu, K. Fu, S. Chowdhury, T. Palacios, and Y. Zhao, IEEE Trans. Electron Devices **68**, 3200 (2021).
[4]T. Pu, U. Younis, H.-C. Chiu, K. Xu, H.-C. Kuo, and X. Liu, Nanoscale Res. Lett. **16**, 101 (2021).
[5]Y. Zhang, A. Dadgar, and T. Palacios, J. Phys. D: Appl Phys. **51**, 273001 (2018).
[6]M. A. Ebrish, M. Porter, A. G. Jacobs, J. C. Gallagher, R. J. Kaplar, B. P. Gunning, K. D. Hobart, and T. J. Anderson, Crystals **12**, 623 (2022).
[7]X. Liu, Q. Liu, C. Li, J. Wang, W. Yu, K. Xu, and J. P. Ao, Jpn. J. Appl. Phys. **56**, 026501 (2017).
[8]T. Oka, Jpn. J. Appl. Phys **58**, SB0805 (2019).
[9]H. Guo *et al.*, Appl. Phys. Rev. **8**, 041405 (2021).
[10]Y. Sun *et al.*, Electronics **8**, 575 (2019).
[11]H. Amano *et al.*, J. Phys. D: Appl Phys **51**, 163001 (2018).
[12]R. Xu *et al.*, IEEE J. Electron Devices **8**, 316 (2020).
[13]S. Liang *et al.*, IEEE Electr. Device Lett. **41**, 669 (2020).
[14]Y. Uemoto, M. Hikita, H. Ueno, H. Matsuo, H. Ishida, M. Yanagihara, T. Ueda, T. Tanaka, and D. Ueda, IEEE Trans. Electr. Devices **54**, 3393 (2007).
[15]L. Yates *et al.*, IEEE Trans. Electron Devices **69**, 1931 (2022).
[16]M. H. Wong, O. Bierwagen, R. J. Kaplar, and H. Umezawa, J. Mater. Res. **36**, 4601 (2021).
[17]R. J. Kaplar, O. Slobodyan, J. D. Flicker, and M. A. Hollis, in *ECS Meeting Abstracts*, Atlanta, GA, Oct. 2019 (IOP, Bristol, UK, 2019), Vol. 31, p. 1334.
[18]A. Barzkar and M. Ghassemi, IEEE Access **8**, 169314 (2020).
[19]Z. Dong, R. Ren, and F. Wang, "Development of high-power bidirectional DC solid-state power controller for aircraft applications," IEEE J. Emerging Sel. Top. Power Electron. (published online).
[20]G. J. Li, X. M. Li, J. L. Zhao, F. W. Yan, Q. X. Zhu, and X. D. Gao, J. Mater. Chem. C **8**, 1125 (2020).
[21]L. A. Li, J. Chen, Z. X. Liu, T. T. Que, X. Gu, L. He, and Y. Liu, Appl. Surf. Sci. **475**, 1043 (2019).
[22]Y. Ren, L. A. Li, N. Y. Liu, K. Zhang, C. G. Li, Z. T. Chen, and B. J. Zhang, Vacuum **182**, 109784 (2020).
[23]J. S. Lee, J. D. Lim, Z. G. Khim, Y. D. Park, S. J. Pearton, and S. N. G. Chu, J. Appl. Phys. **93**, 4512 (2003).
[24]K. Nie *et al.*, IEEE Electr. Device Lett. **41**, 469 (2020).
[25]X. Li, T. Pu, T. Zhang, X. Li, L. Li, and J. P. Ao, IEEE Sens. J. **20**, 62 (2020).
[26]Y. Wang, T. Pu, X. Li, L. Li, and J. P. Ao, Mater. Sci. Semicond. Proc. **125**, 105628 (2021).
[27]J. Zhou, L. He, X. Li, T. Pu, L. Li, and J. P. Ao, Superlattice Microstruct. **151**, 106820 (2021).
[28]L. Li, A. Kishi, T. Shiraishi, Y. Jiang, Q. Wang, and J.-P. Ao, J. Vac. Sci. Technol. A **32**, 02B116 (2014).
[29]T. D. Desissa, Ceram. Int. **47**, 8053 (2021).
[30]R. K. Gupta, K. Ghosh, and P. K. Kahol, Physica E **41**, 617 (2009).
[31]P. K. Das, R. Biswal, R. J. Choudhary, S. A. Khan, R. C. Meena, N. C. Mishra, and P. Mallick, Mater. Res. Express **6**, 106413 (2019).

Published under an exclusive license by the AVS

[32]A. Merih Akyuzlu, F. Dagdelen, F. Yakuphanoglu, A. Gultek, and A. A. Hendi, Eur. Phys. J. Plus **132**, 178 (2017).
[33]Y. Kokubun, S. Kubo, and S. Nakagomi, Appl. Phys. Express **9**, 091101 (2016).
[34]A. J. Green *et al.*, APL Mater. **10**, 029201 (2022).
[35]S. J. Pearton, F. Ren, M. Tadjer, and J. Kim, J. Appl. Phys. **124**, 220901 (2018).
[36]C. Wang *et al.*, J. Phys. D: Appl. Phys. **54**, 243001 (2021).
[37]W. Xiong *et al.*, IEEE Electr. Device Lett. **42**, 430 (2021).
[38]M. Xiao *et al.*, IEEE Trans. Power Electr. **36**, 8565 (2021).
[39]X. Lu, X. Zhou, H. Jiang, K. W. Ng, Z. Chen, Y. Pei, K. M. Lau, and G. Wang, IEEE Electr. Device Lett. **41**, 449 (2020).
[40]Q. Yan *et al.*, Appl. Phys. Lett. **118**, 122102 (2021).
[41]H. H. Gong *et al.*, Appl. Phys. Lett. **118**, 202102 (2021).
[42]W. Hao *et al.*, Appl. Phys. Lett. **118**, 043501 (2021).
[43]F. Zhou *et al.*, IEEE Trans. Power Electr. **37**, 1223 (2022).
[44]Q. Yan *et al.*, Appl. Phys. Lett. **120**, 092106 (2022).
[45]T. Zhang, L. Wang, X. Li, Y. Bu, T. Pu, R. Wang, L. Li, and J.-P. Ao, Appl. Surf. Sci. **462**, 799 (2018).
[46]K. Baraik, S. D. Singh, Y. Kumar, R. S. Ajimsha, P. Misra, S. N. Jha, and T. Ganguli, Appl. Phys. Lett. **110**, 191603 (2017).
[47]L. Li, W. Wang, L. He, X. Zhang, Z. Wu, and Y. Liu, J. Alloys Compd. **728**, 400 (2017).
[48]J. A. Spencer, A. L. Mock, A. G. Jacobs, M. Schubert, Y. Zhang, and M. J. Tadjer, Appl. Phys. Rev. **9**, 011315 (2022).
[49]E. A. Kraut, R. W. Grant, J. R. Waldrop, and S. P. Kowalczyk, Phys. Rev. Lett. **44**, 1620 (1980).
[50]G. Greczynski and L. Hultman, Appl. Surf. Sci. **451**, 99 (2018).
[51]Z. Feng *et al.*, Adv. Electron. Mater. **7**, 2100414 (2021).
[52]C. Fares, F. Ren, Max Knessl, H. von Wenckstern, M. Grundmann, and S. J. Pearton, "Chapter 9," in *Wide Bandgap Semiconductor Based Electronics*, edited by F. Ren and S. J. Pearton (IOP Publishing, Bristol, 2020).
[53]D. C. Hays, B. P. Gila, S. J. Pearton, and F. Ren, Appl. Phys. Rev. **4**, 021301 (2017).

Published under an exclusive license by the AVS